PROCEEDINGS

of the

LASER MATERIALS PROCESSING CONFERENCE

ICALEO'93

LIA Volume 77

CO-CHAIRS:

Paul Denney, Pennsylvania State University, USA

Isamu Miyamoto, Osaka University, Japan

B.L. Mordike, Technische Universitat Clausthal, Germany

Published by the LIA

Laser Institute of America
12424 Research Parkway, Suite 125
Orlando, FL 32826

DYNAMICS OF MELTING AND EVAPORATION IN PULSED LASER DEPOSITION: NUMERICAL SIMULATION

V.I. MAZHUKIN
Institute of Mathematical Modeling, Russian Academy of Sciences, Miusskaya square, 4, 125047 MOSCOW, Russia

I. SMUROV
Ecole Nationale d'Ingénieurs de SAINT-ETIENNE
58, Rue Jean Parot, 42023 SAINT-ETIENNE Cedex 2, France

G. FLAMANT
Institut de Science et de Génie des Matériaux et Procédés, C.N.R.S;, B.P. 5, 66125 FONT-ROMEU Cedex, France

1. MATHEMATICAL MODEL

Mathematical description of the processes of laser heating, melting-solidification and evaporation of superconducting ceramics is made within the framework of the combined version of the Stefan problem including the dynamics of both phase fronts : melting-solidification and evaporation. The proposed mathematical model is a boundary-value problem for the thermal conductivity equation with two moving phase boundaries solid-liquid $\Gamma_{sl}(t)$ and liquid-vapour $\Gamma_{lv}(t)$. Volume heating of the solid and liquid phases is taken into account with the help of the term $\partial G/\partial x$ in the heat transfer (1) and the radiation transfer (2) equations

$$\left[C_p(T)\,\rho \frac{\partial T}{\partial t} = \frac{\partial}{\partial x} \lambda(T) \frac{\partial T}{\partial x} - \frac{\partial G}{\partial x} \right]_k \qquad (1)$$

$$\left[\frac{\partial G}{\partial x} + \kappa G = 0 \right]_k, \quad k = s, l \qquad (2)$$

solid phase : $x_0 < x < \Gamma_{sl}(t)$,

liquid phase : $\Gamma_{sl}(t) < x < \Gamma_{lv}(t)$, $\quad t > 0$

boundary condition : $x = x_0, \quad \lambda \dfrac{\partial T}{\partial x} = 0$

In the classical version of the Stefan problem for the description of melting-solidification phase transitions at the interphase boundary $\Gamma_{sl}(t)$ the differential condition is used

$$x = \Gamma_{sl}(t) : \quad \lambda_s \frac{\partial T_s}{\partial x} - \lambda_l \frac{\partial T_l}{\partial x} = \rho_s L_m v_{sl} \qquad (3)$$

$$T_{sl} = T_s = T_l = T_m \qquad (4)$$

from which the velocity of the front movement v_{sl} is

determined.

Intensive evaporation gives rise to a strongly nonequilibrium Knudsen layer at the interface. In the present paper the relations reported in [1] are used. In case of volume heating of a condensed medium the boundary conditions on the surface being evaporated have the form :

$$x = \Gamma_{lv} : \quad -\lambda_{sr}\frac{\partial T_{sr}}{\partial x} = \varrho_{sr} L_v \upsilon_{lv} + \sigma T^4_{sr}, \tag{6}$$

$$\varrho_{sr}\upsilon_{lv} = \varrho_v(\upsilon_{lv} - u), \tag{7}$$

$$P_{sr} + \varrho_{sr}\upsilon^2_{lv} = P_v + \varrho_v(\upsilon_{lv} - u)^2, \tag{8}$$

$$T_v = T_{sr}\left[\left[1 + f^2\left|\frac{\gamma - 1}{\gamma + 1}\right|M^2\right]^{1/2} - f\left|\frac{\gamma - 1}{\gamma + 1}\right| M\right|^2, \tag{9}$$

$$\varrho_v = \frac{1}{2}\varrho_H\left\{\left|\frac{T_{sr}}{T_v}\right|^{1/2}\left[(\gamma M^2 + 1)\exp(b^2M^2)\,\mathrm{erfc}(bM) - \frac{4f}{\pi}M\right] + \frac{T_{sr}}{T_v}\left[1 - 2.f.M\exp(b^2M^2)\,\mathrm{erfc}(bM)\right]\right|, \tag{10}$$

$$M = u/u_c, u_c = (\gamma R T_v)^{1/2}, \; b = (\gamma/2)^{1/2}, \; f = (\pi.\gamma/8)^{1/2},$$

$$\varrho_H = P_H T_{sr}/(R T_{sr}), \; P_H = p_b \exp\left|\frac{L_v}{R T_{sr}}\left|1 - \frac{T_b}{T_{sr}}\right|\right|$$

$$G_{sr} = A(T_{sr})\, G_o \exp\left[-\left|\frac{t}{\tau}\right|^2\right]$$

Nomenclature : a - thermal diffusivity; $A(T_{sr})$- surface absorptivity; C_p - heat capacity; G - energy density flux; G_0 - maximum value of incident energy density flux; L_m - latent heat of melting; L_V - latent heat of evaporation; M - Mach number; P - pressure; R - universal gas constant; T_0 - initial temperature; T_m - melting point; u - vapor velocity; υ_{sl} - velocity of solid - liquid interface; υ_{lv} - velocity of liquid-vapor interface; γ - the ratio of heat capacities; Γ_{sl} - solid-liquid interface; Γ_{lv} - liquid-vapor interface; $\varkappa$ - coefficient of heat conductivity; ϱ - density.

Subscripts : b - boiling point; H - saturated vapor; l - liquid phase; s - condensed phase; v - gas phase; sr - surface.

2. Results and Discussion

According to the $\varkappa(\lambda v)$ curve based on experimental data [2], the absorption coefficient $\varkappa$ ranges from $\varkappa = 8.10^5 \cdot cm^{-1}$

for the radiation wavelength $\lambda v = 0.2$ μm to $\varkappa = 10^4$ cm^{-1} for the radiation wavelength $\lambda v \geq 1$ μm. Thus, depending on the incident radiation wavelength λv, superconducting ceramics can absorb either practically as metals (surface heating) or as dielectrics (the volume mechanism of energy release). It is evident that the variation of the laser radiation dissipation mechanism must lead to qualitative changes in basic processes.

The parameters were chosen to be the typical ones for PLD regimes of thin superconducting films deposition. The temporal profile of laser pulse was assumed to have the Gaussian shape with respect to the variable t :

$$G(t) = G_0 \exp(-(t/\tau)^2)$$

where $-\infty < t < +\infty$, τ is the pulse half-width at the half-height, $\tau = 40$ ns, G_0 is the maximum intensity, $G_0 = 10^7$ W/cm^2. In the present simulation G_0 and τ remain the same for all the variants.

Heat transfer and optical properties of the solid phase were taken to be independent of temperature and the values were chosen in accordance with experimental data [2-4] :

$A = 0.8$, $T_m = 1300$ K, $T_V = 2000$ K, $C_P = 0.5$ J/g K,

$L_m = 2.5\ 10^2$ J/g, $L_V = 6\ 10^3$ J/g, $\lambda_s = 3\ 10^{-2}$ W/cm K

2.1 TEMPERATURE DISTRIBUTION. Under the combined action of the processes of melting and volume heating, the temperature maximum, fig. 1, is formed in subsurface layers of the material. The presence of the subsurface temperature maximum indicates that a certain volume of the solid phase is overheated with respect to the melting equilibrium temperature T_m. Liquid phase heating causes an intensive surface evaporation, which in turn (with allowance for volume energy release in the depth of the liquid phase) leads to the formation of the second temperature maximum. When a certain relation between the parameters is respected, both maxima can be observed simultaneously, fig.2.

At the same time owing to the accumulation of energy in the subsurface layer the processes of melting-solidification and evaporation become extended in time. Thus, intensive evaporation begins after passing the maximum G(t) and continues when the intensity G(t) decreases by more than one order. As a result, the profiles of the rate $\upsilon_{lv}(t)$, fig.4, and pressure $P_{sr}(t)$ are shifted to the right with respect to the intensity maximum.

2.2 GENERAL TENDENCIES. To show general tendencies of the dynamics of phase transitions, laser action over a wide range of mean free paths $lv \sim \varkappa^{-1}$ (from $lv = 0$ to $lv = 5.10^3$ A) was analysed.

In the case of surface action $lv = 0$ the highest evaporation rates $|U^{max}_{lv}| \approx 1.5$ m/s, fig.5, and the highest solidification rates $|U^{max}_{sl}| \approx 2$ m/s, fig.8, are found, and the strongest ejection of the material due to evaporation $x^{max}_v \approx 800$ A, fig.6, is observed. Melting has the lowest rate, fig.8. The ratio of these rates determines the melt thickness, fig.7, and the lifetime of the liquid phase.

The maximum values of volume overheating temperatures

for the solid and liquid phases $\Delta T^{max}_{s,l}$ (fig.9); and lifetime $\Delta t^{ex}_{s,l}$ (fig.10) are calculated. All the values which characterize the overheating of the solid phase have a tendency to increase with increasing lv (figs.9-10). The maximum values are reached when $\varkappa v = 5\ 10^4\ cm^{-1}$: $\Delta T^{max}_s \approx 155K$, $\Delta t_s \approx 60$ ns. In experiments an explosive decay of the metastable state in solid phase can lead to an ejection of solid phase (particles) of the material.

At the same time the increase of the energy releasing area causes a reduction of the evaporation rate U_{lv}, fig.5. Thus, two main parameters forming the volume overheating of the liquid phase act in the opposite directions. All the dependencies (figs.9-10) describing the volume overheating of the liquid ΔT^{max}_l (lv), Δt^{ex}_l (lv) in the range of lv = 1000 - 3000 A pass through the extreme values : ΔT^{max}_l (lv = 1000 A) $\approx$ 400K, Δt^{ex}_l (lv = 1500 A) $\approx$ 140 ns. So, high values of the temperature ΔT^{max}_l and the lifetime Δt^{ex}_l of the overheating increase greatly the probability of an explosive decay of the metastable phase. In experiments this effect can occur as an ejection of material in the form of droplets.

3. CONCLUSION

The numerical simulation shows that pulsed laser evaporation of materials with a volume energy release may lead to volume overheating of the solid and liquid phases. The maximum values of the overheating of the solid phase exceed a hundred degrees and those for the liquid phase exceed several hundreds degrees. The times of the metastable states existence are tens and hundreds nanoseconds, respectively. The metastability of the solid phase leads to the domination of the melting process which, together with a decreased effect of evaporation and low solidification rates, makes the liquid phase lifetime 5-6 times longer than for the surface absorption of radiation. It is shown that the probability of explosive decay of the metastable states in solid phase increaces with laser wavelength, while for the ones in the liquid phase the corresponding dependencies have the maxima versus laser wavelength.

References

1. C.J. Knigt, AIAA Journal, v.17, N°5, pp 519-523.
2. E. Fogarassy, C. Fuchs, S. de Unamuno, J. Perriere, F. Kerherve., (1992), Materials and Manufacturing Processes, 7, 31.
3. R. K. Williams, R.S. Graves, D.M. Kroeger, G.C. Marsh, and J.O. Scarbrough, J. Brynestad., (1989),J. Appl. Phys., 66 (12), pp 6181-6184.
4. J. Orenstein, G.A. Thomas, F.J. Millis, S.L. Cooper, D.H. Rapkine, T. Timusk, L.f. Schneemeyer and J.V. Waszczak. Crystals. (1990) Phys. Rev. B. (1990), vol. 42, pp 6342-6362.

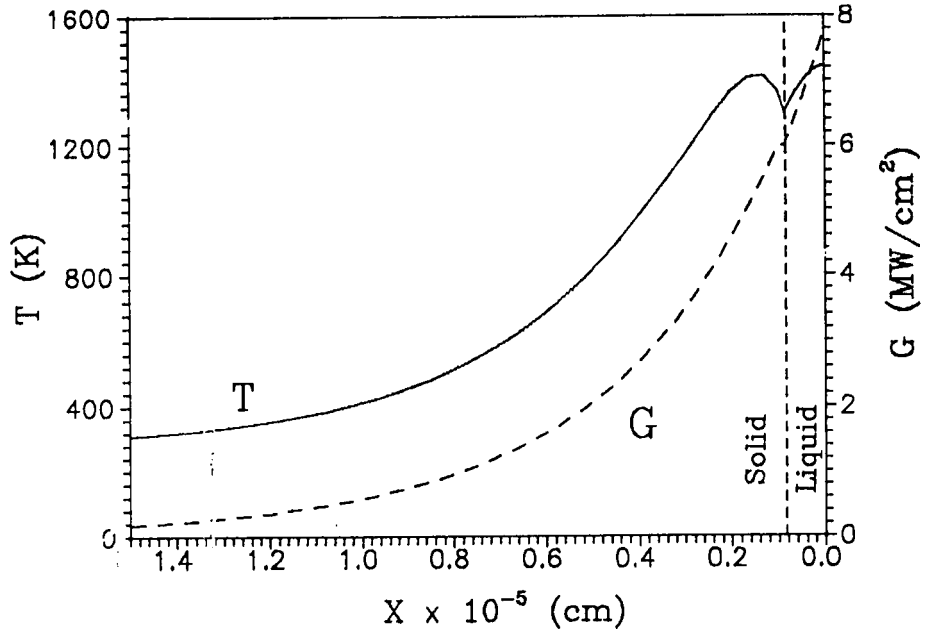

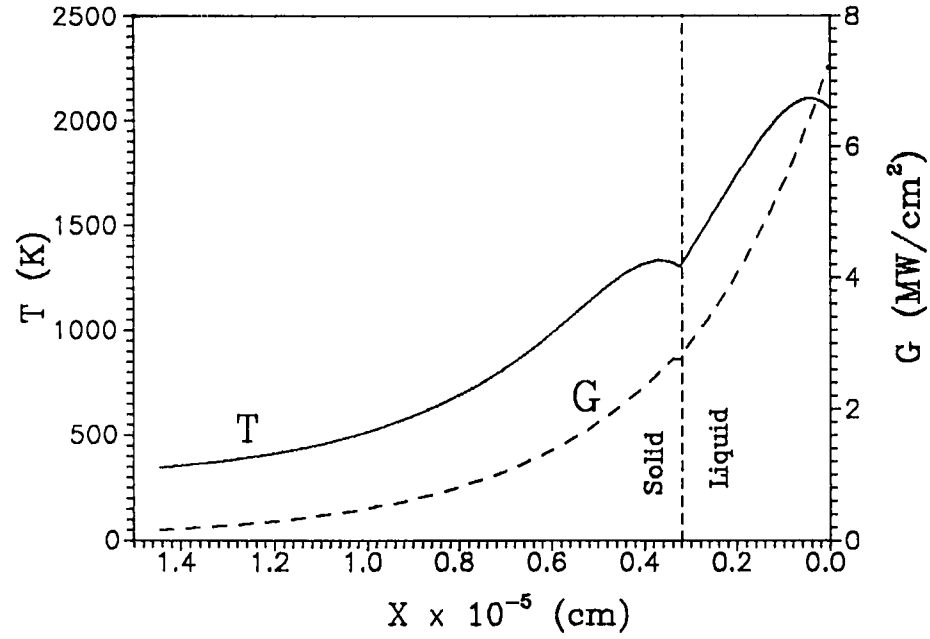

Fig.1. Spatial distribution of temperature T and absorbed energy intensity G illustrating the appearance of solid state overheating short time after the melting starts (l_V=3000 A).

Fig.2. Spatial distribution of temperature T and absorbed energy intensity G illustrating the existance of two subsurface temperature maxima, short time after the intensive evaporation starts (l_V=3000 A).

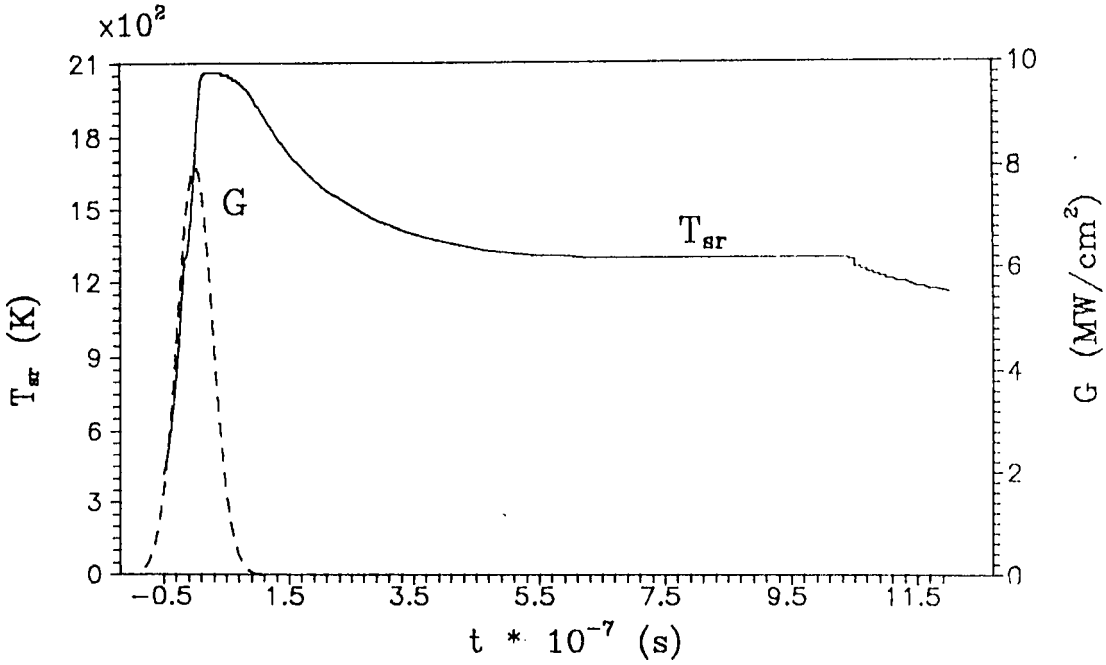

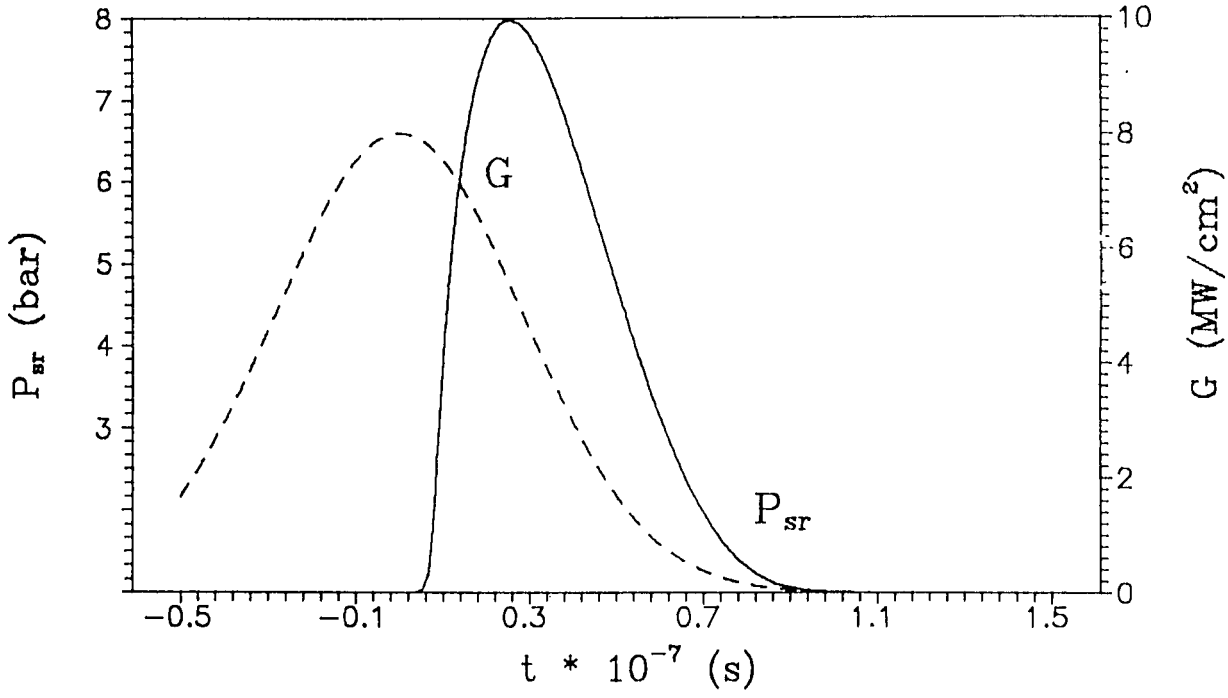

Fig. 3. Surface temperature T_{sr} and laser pulse intensity G versus time (l_V=3000 A).
Fig. 4. Recoil reactive pressure P_{sr} and laser pulse intensity G versus time (l_V=3000 A).

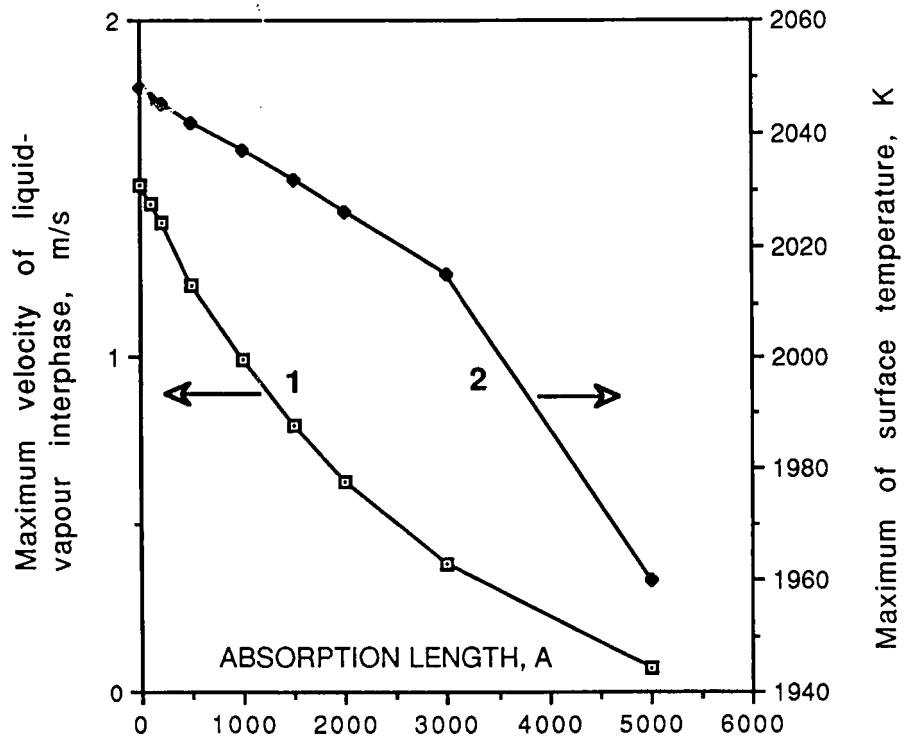

Fig. 5. Maximum values of surface temperature (1) and evaporation front velocity (2) during thermocycle versus absorption length.

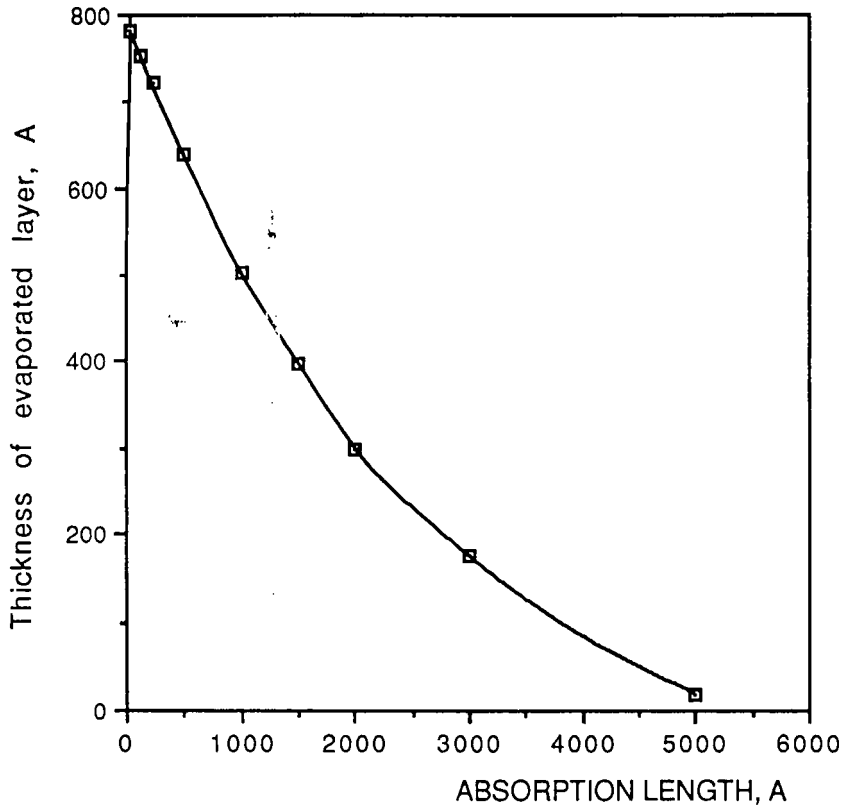

Fig.6. Thickness of evaporated layer versus absorption length.

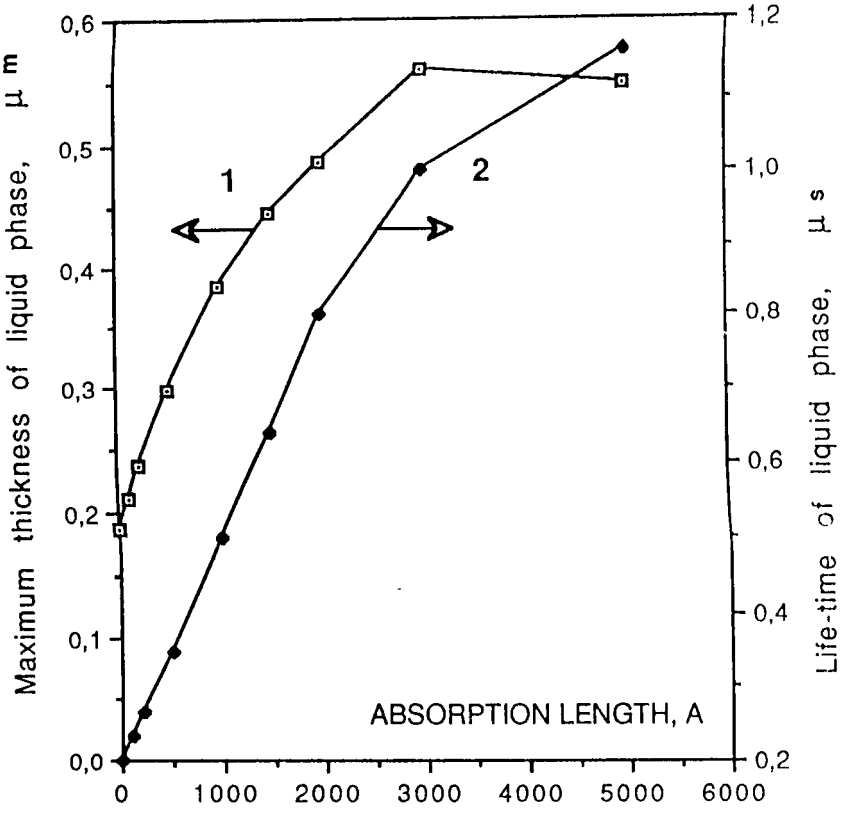

Fig. 7. Maximum thickness of liquid phase (1) and its life-time (2) versus absorption length.

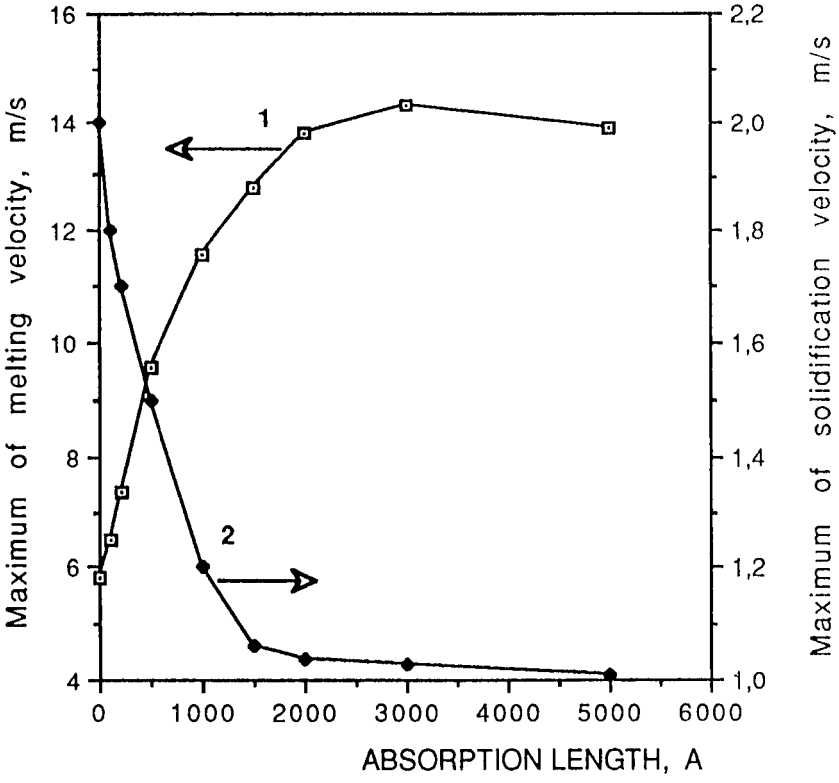

Fig.8. Maximum values of melting (1) and solidification (2) velocities (during thermocycle) versus absorption length.

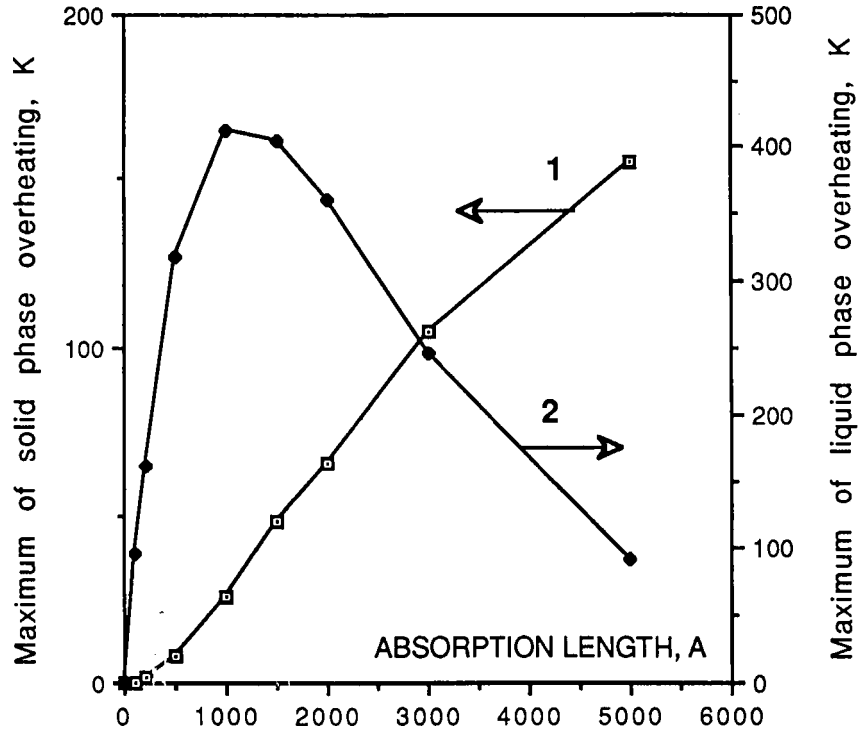

Fig.9. Maximum values of solid (1) and liquid (2) phase overheating versus absorption length.

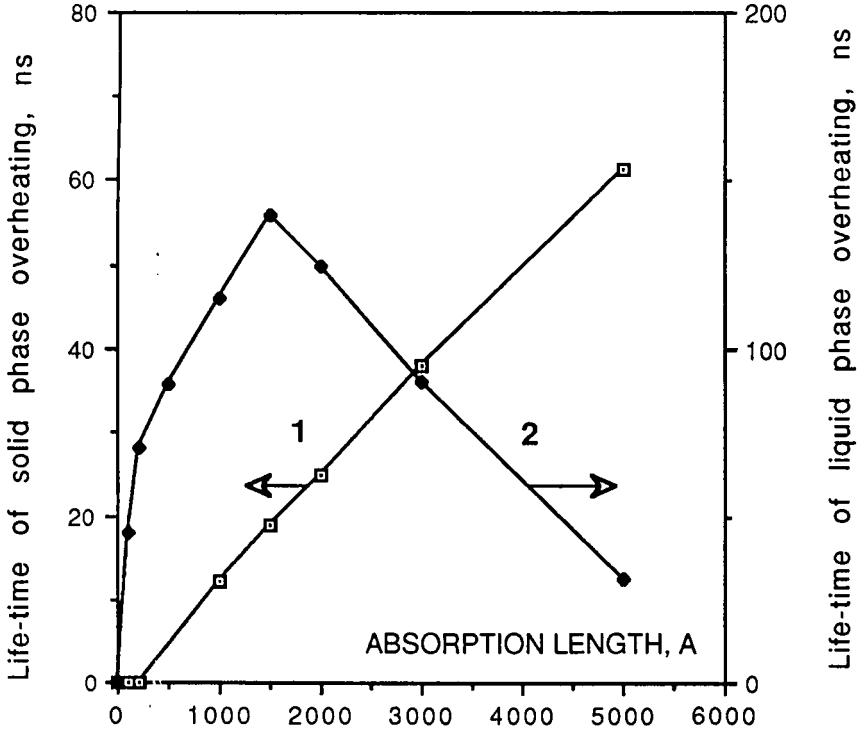

Fig.10. Life-time of solid (1) and liquid (2) phase overheating versus absorption length.